Journal of Materials Chemistry B

ROYAL SOCIETY OF CHEMISTRY

PAPER

View Article Online
View Journal | View Issue

Cite this: J. Mater. Chem. B, 2023, 11, 8775

In vitro evaluation of granules obtained from 3D sphene scaffolds and bovine bone grafts: chemical and biological assays†

Stefano Sivolella,*[a] Giulia Brunello,[ab] Ervin Nika,[a] Denis Badocco,[c] Paolo Pastore,[c] Sara M. Carturan,[de] Enrico Bernardo,[f] Hamada Elsayed,[fg] Lisa Biasetto[h] and Paola Brun[i]

Sphene is an innovative bone graft material. The aim of this study was to investigate and compare the physicochemical and biological properties of Bio-Oss® (BO) and in-lab synthesized and processed sphene granules. BO granules of 1000–2000 μm (BO-L), 250–1000 μm (BO-S) and 100–200 μm (BO-p) for derived granules, and corresponding groups of sphene granules obtained from 3D printed blocks (SB-L, SB-S, SB-p) and foams (SF-L, SF-S and SF-p) were investigated. The following analyses were conducted: morphological analysis, specific surface area and porosity, inductively coupled plasma mass spectrometry (ICP-MS), cytotoxicity assay, Alizarin staining, bone-related gene expression, osteoblast migration and proliferation assays. All pulverized granules exhibited a similar morphology and SF-S resembled natural bone. Sphene-derived granules showed absence of micro- and mesopores and a low specific surface area. ICP-MS revealed a tendency for absorption of Ca and P for all BO samples, while sphene granules demonstrated a release of Ca. No cellular cytotoxicity was detected and osteoblastic phenotype in primary cells was observed, with significantly increased values for SF-L, SF-S, BO-L and BO-p. Further investigations are needed before clinical use can be considered.

Received 8th March 2023,
Accepted 27th August 2023

DOI: 10.1039/d3tb00499f

rsc.li/materials-b

1. Introduction

The treatment of alveolar bone defects in oral and periodontal surgery often requires bone graft materials; their origin and shape can be autologous, homologous, heterologous and synthetic, in granules or blocks. Heterologous bone substitutes are widely employed in dentistry owing to their high biocompatibility, unlimited availability and reduced morbidity.[1] Nevertheless, there is a growing demand for non-animal alternatives due to ethical and religious concerns.[2,3] Furthermore, the development of synthetic bone substitutes in conjunction with digital modern manufacturing technologies has recently attracted increasing interest due to the high possibility of customization to meet the specific application needs.[4,5]

Among the synthetic materials, a new class of silica-based bioceramics has recently gained a significant interest.[6–8] In particular, sphene ($CaOTiO_2SiO_2$) can be synthesized for biomedical applications according to the polymer-derived ceramics process (PDC) because of its high chemical stability and cytocompatibility.[9] The PDC offers numerous advantages in terms of shaping possibilities, from bulk components to scaffolds with interconnected pore structures, and allows the development of high purity crystalline phases.[9,10] *In vitro* studies have shown that sphene can promote the adhesion, proliferation, and osteogenic differentiation of primary cells derived from human bone.[11] In addition, in human primary osteoblasts, sphene induces the up-regulation of genes involved in osteoblastic differentiation, such as alkaline phosphatase (ALP), bone sialoprotein (BSP), and type 1 collagen.[12] Sphene

[a] Department of Neuroscience, Dentistry Section, University of Padova, Via Giustiniani 2, 35128 Padova, Italy. E-mail: stefano.sivolella@unipd.it, giulia.brunello@unipd.it, nkirvn@unife.it
[b] Department of Oral Surgery, Universitätsklinikum Düsseldorf, Moorenstr. 5, 40225 Düsseldorf, Germany
[c] Department of Chemical Sciences, University of Padova, Via F. Marzolo 1, 35131 Padova, Italy. E-mail: denis.badocco@unipd.it, paolo.pastore@unipd.it
[d] INFN-Laboratori Nazionali di Legnaro, Viale dell'Università 2, 35020, Legnaro, PD, Italy. E-mail: saramaria.carturan@unipd.it
[e] Dipartimento di Fisica e Astronomia, Università di Padova, Via Marzolo 8, 5131, Padua, Italy
[f] Department of Industrial Engineering, University of Padova, Via F. Marzolo 9, 35131 Padova, Italy. E-mail: enrico.bernardo@unipd.it, hamada.elsayed@unipd.it
[g] Refractories, Ceramics and Building Materials Department, National Research Centre, El Buhouth Str., Cairo 12622, Egypt
[h] Department of Management and Engineering, University of Padova, Stradella San Nicola 3, 36100 Vicenza, Italy. E-mail: lisa.biasetto@unipd.it
[i] Department of Molecular Medicine, Section of Microbiology, University of Padova, via A. Gabelli, 63, 35121 Padova, Italy. E-mail: paola.brun.1@unipd.it

† Electronic supplementary information (ESI) available. See DOI: https://doi.org/10.1039/d3tb00499f

has been demonstrated to foster the osteoblastic differentiation of human stem cells derived from adipose tissue.[13] The induction of osteocalcin gene expression by sphene suggests a good potential in promoting the mineralization of the extracellular matrix. These promising *in vitro* findings have been confirmed *in vivo*, by the successful osseointegration of sphene-coated titanium implants in different animal models.[12,14] The favourable biological properties of this silica-based ceramic could be related to the slow release of silicon ions into the surrounding environment, which is deemed to stimulate the osteoblast activity and enhance the production of collagen, a key component of bone tissue.[15] Deproteinized bovine bone matrix (DBBM) is one of the most investigated graft materials for bone regeneration; it is commercially available in granules of different sizes, ranging from 250 to 1000 μm (small-S) and from 1000 to 2000 μm (large-L).[16–24] The size and geometry of bone graft materials are deemed to play a crucial role during wound tissue healing. Indeed, particle size and porosity could influence the osteoconductive properties and the degradation kinetics of the biomaterials.[25] Smaller particles can be incorporated into paste-like injectable formulations and enable an easy handling.[26,27] A *trans*-mucosal migration of grafted granules has been observed following preservation of extraction sockets;[28,29] it may induce inflammation of the mucosa of the grafted sites.[30,31] However, it has been reported that exfoliation of smaller particles might be less harmful to periodontal/peri-implant tissues.[32]

A canine animal model showed that the osteoconductive properties of granules issued from pulverized DBBM in the 125–250 μm range were comparable to those observed with larger commercially available granules made of the same material.[27] In another preclinical porcine calvarial bone defect model, the same DBBM in an injectable paste form, composed of granules of 250–500 μm and a carrier of carboxymethylcellulose and collagen, supported new bone formation and maintained volumetric stability.[26]

So far and to the best of our knowledge, there is no study that focused on the application of sphene granules as a bone grafting material. Therefore, this *in vitro* study aimed to evaluate and compare the physico-chemical and biological properties of sphene and DBBM large, small and pulverized granules. Further antimicrobial properties of the biomaterials were investigated and reported as ESI.†

2. Experimental section

2.1. Biomaterials

Deproteinized bovine bone matrix (DBBM) granules (Bio-Oss®, Geistlich Biomaterials, Wolhusen, Switzerland) were purchased from the local distributor in the commercialized forms large (L, granule size 1000–2000 μm) and small (S, granule size 250–1000 μm). This biomaterial is a chemically and thermally treated cancellous bovine bone. Grinded bovine bone is first deproteinized by reaction with the strong alkali medium and then calcined at 300 °C.

From Bio-Oss® L (BO-L) and S (BO-S) particles, smaller granules of 100–200 μm (pulverized, p), BO-Lp and BO-Sp respectively, were obtained through mechanical shredding using sterile stainless steel tools, and the subsequent use of 2 consecutive cylindrical sterile stainless steel sieves of Ø 6 cm and mesh sizes of 200 μm and 100 μm, respectively (Filtra Vibraciòn, Badalona, Spain).

Sphene granules were obtained by a similar shredding process starting from 1 cm × 1 cm × 0.2 cm blocks of 3D printed sphene and sphene foams.

Sphene blocks were 3D printed using Direct Ink Writing (DIW) technology. Briefly, the ink was developed according to the stoichiometric 1/1/1 molar ratio between $CaO/TiO_2/SiO_2$, starting from commercially available precursors. In particular, preceramic silicone polymer (SILRES® MK, polymethylsiloxane, Wacker-Chemie GmbH, Munich, Germany) and fumed silica (FS, Aerosil R106, Evonik Germany) were used as silica precursors, with 84% by weight the ceramic yield of MK when treated in air.[9] Calcium carbonate ($CaCO_3$, 10 μm, Industrie Bitossi, Vinci, Italy), and titanium oxide (TiO_2, 21 nm, Evonik Degussa GmbH, Germany) were the sources of CaO and TiO_2, respectively. The MK silicone and fumed silica were first dissolved in isopropanol alcohol (28 vol%), using a planetary mixer (THINKY ARE-250, Intertronics, UK), for 3 min at 1200 rpm. Calcium carbonate and titanium oxide powders were added to the silicone solution. The ink was homogenized by the planetary mixer for 3 min at 1200 rpm and then for 3 min at 2000 rpm; it was followed by a defoaming step for 3 min at 2000 rpm. The 3D sphene parts were fabricated by extruding the filaments (diameter of ~410 μm) crossed perpendicularly to each other and with a spacing between them of 800 μm. The scaffolds were subsequently sintered using reactive sintering up to 1300 °C in air as previously described in Elsayed *et al.*[9] After shredding, the granules derived from 3D printed sphene blocks were separated through 4 consecutive steel sieves with mesh sizes of 2000 μm, 1000 μm, 200 μm and 100 μm assembled in sequence to obtain Sphene Block-L (SB-L, 1000–2000 μm), Sphene Block-S (SB-S, 200–1000 μm) and Sphene Block-p (SB-p, 100–200 μm) granules.

The same procedure was applied to sphene foam blocks that were produced by direct foaming of a silicone-fillers paste (*i.e.* the paste used for the DIW process) to create scaffolds with a stochastic interconnected pore architecture. The paste was manually cast into cylindrical molds and subjected to direct foaming by heating 5 °C min^{-1} up to 350 °C in the air for 30 min, using, an hydrazine derivative (HZ; *N*′-dicarbamoylhydrazine, or biurea; $C_2H_6N_4O_2$, 98%, Alfa Aesar, UK) as a foaming agent (1 wt%) that was added to the slurry and mixed.[10] The foams were later heat-treated at 1300 °C for 3 h in the air with a heating rate of 1 °C min^{-1}, to develop the desired sphene ceramic foams. Large (SF-L, 1000–2000 μm), small (SF-S, 200–1000 μm) and pulverized (SF-p, 100–200 μm) granules were then obtained with the above described crushing and sieving method. Ten groups of samples were obtained and analyzed as reported in Table 1. Commercially available BO-L and BO-S were provided sterile, while for the biological

Table 1 List of materials utilized in the study and their labelling

	Granule size (μm)		
Granule origin	1000–2000 (L)	200–1000 (S)	100–200 (p)
DBBM large granules	BO-L	—	BO-Lp
DBBM small granules	—	BO-S	BO-Sp
3D printed sphene block	SB-L	SB-S	SB-p
Sphene foam block	SF-L	SF-S	SF-p

DBBM: deproteinized bovine bone matrix; BO: Bio-Oss®; SB: 3D printed sphene blocks; SF: sphene foam blocks; L: large granules; S: small granules; p: pulverized granules (BO-Lp and BO-Sp: pulverized granules from BO-L and BO-S, respectively).

tests BO-p and sphene granules were sterilized by steam autoclaving.

2.2. Morphological characterization

Micrographs were acquired using an environmental scanning electron microscope (FEI ESEM Quanta 200 Company, Hillsboro, OR, US). The images were collected at a working distance of 15 mm at an acceleration of 20 kV at increasing magnifications of 25×, 100× and 1000×. At least two images per group were taken. The low vacuum mode allowed the observation without requiring a gold or other conductive coating.

The qualitative analysis of the chemical composition of the biomaterials was performed by an energy dispersion spectrometry (EDS) detector (EDAX Genesis, EDAX Inc., Mahwah, NJ, US) at solid state. The acquisition of the obtained signal was performed for 50 s, operating at 20 kV.

2.3. Specific surface area and porosity analysis

The specific surface area (SSA), the porosity vol% and the pore size distribution (PSD) of the granules were determined by N_2 physisorption at 77 K (ASAP Model 2020, Micromeritics, Norcross, GA, USA). The specific surface area was determined using the BET equation, while the total pore volume was derived as the total amount of N_2 adsorbed at P/P_0 = 0.98. The pore size distribution was obtained using the Barrett–Joyner–Halenda (BJH) model applied to the desorption branch, while the micropore volume was estimated using the *t*-plot method. Prior to the analysis, each sample was degassed under vacuum for 10 hours at 350 °C. The pores were classified according to their size with reference to the IUPAC nomenclature in macropores (>50 nm), mesopores (2–50 nm) and micropores (<2 nm).[33] The micropore size distribution was derived using the Horwath–Kawazoe model.

2.4. Inductively coupled plasma mass spectrometry (ICP-MS)

Samples for ICP-MS analysis were prepared by incubating 8 mg of each biomaterial in 2 mL of complete, cell-free Dulbecco's Modified Eagle Medium (D-MEM)/F12 in 6-well culture plates. Samples were incubated for 24 hours, 7 days or 14 days at 37 °C and 5% CO_2 in a humidified incubator and under constant shaking. At the end of the incubation time, the culture media were centrifuged (2500 rpm, 10 minutes) and filtered with 0.22 μm polytetrafluoroethylene (PTFE) syringe filters (Millipore Corporation, Bedford, MA, USA) to avoid the presence of biomaterial particles in the analyzed solution. Then, 0.5 mL of sample were diluted to 8.0 mL with milliQ water. A blank sample, used as a control, was prepared by adding 7.5 mL of milliQ water to 0.5 mL of complete D-MEM/F12 culture medium incubated for 14 days under the conditions described above but without biomaterials.

An Agilent 7700× ICP-MS instrument was used for the measurements (Agilent Technologies International Japan, Ltd, Tokyo, Japan). The instrument is equipped with an octupole collision cell operating in kinetic energy discrimination mode, which was used for the removal of polyatomic interferences and argon-based interferences. The ICP-MS was tuned daily using a tuning solution containing 1 μg L^{-1} ^{140}Ce, ^{7}Li, ^{205}Tl, and ^{89}Y (Agilent Technologies, UK). The internal standard (IS) mixture (Agilent, 5183-4681) containing ^{6}Li, ^{45}Sc, ^{72}Ge, ^{103}Rh, ^{115}In, ^{159}Tb, ^{175}Lu and ^{209}Bi at 10 μg mL^{-1} each in 3.5% HNO_3 was used through addition to the sample solution *via* a T-junction. The matrix effect was tested by spiking the blank solution with the multi-standard solutions. The IS was adopted to correct both the matrix and drift effects.

The detection limits of the analytical procedure are: 2.9 μg mL^{-1} for Ca, 2.3 μg mL^{-1} for P, 2.1 μg mL^{-1} for K, 1.8 μg mL^{-1} for Na, 0.006 μg mL^{-1} for Ti, 12 μg mL^{-1} for Si and, 0.2 μg mL^{-1} for Mg.

For multi-element calibration, all solutions were prepared in milliQ ultrapure water obtained with a Millipore Plus System (Milan, Italy, resistivity 18.2 MOhm cm^{-1}). Multi-element standard solutions for calibration were prepared in HNO_3 3.5% by gravimetric serial dilution at six different concentrations (min. 1 μg L^{-1} max^{-1}. 10 mg L^{-1}) for IMS-120 and CCS-5 multi-element calibration standard. The reported values are normalized to the potassium concentration values measured in the control solution. All regressions were linear with a determination coefficient (R^2) larger than 0.9998. The stability of the calibration curve was tested periodically by re-measuring the standard solutions. All measurements were repeated in duplicate.

- CCS-5 (Inorganic-Ventures) Multistandard, 100 mL: 100.00 ± 0.70 μg mL^{-1} of B, Ge, Hf, Mo, Nb, P, Re, S, Sb, Si, Sn, Ta, Ti, W and Zr: matrix HNO_3 7.14% + 1% HF v/v.
- IMS-120. (Ultra Scientific Multistandard) Multistandard, 100 mL: in 5% HNO_3 with trace HF. 10 mg L^{-1} of Ag, Al, As(100), B(100), Ba, Be(100), Bi, Ca(1000), Cd, Co, Cr, Cu, Fe(100), Ga, K, Li, Mg, Mn, Mo, Na, Ni, Pb, Rb, Se(100), Sr, Te, Tl, U, V and Zn(100).
- HNO_3 69% CAS 7697-37-2. (Sigma Aldrich).

2.5. Primary human osteoblast culture

Primary human osteoblasts were obtained from leftover cortical mandible bone collected from a 39 years old male during deeply impacted third molar extractions (research protocol No. 4899/AO/20 Ethics Committee Azienda Ospedaliera/Università di Padova). Bone fragments were initially cultured in D-MEM/F12 (1 : 1) supplemented with 20% v/v fetal bovine serum, 1% v/v sodium pyruvate, 1% v/v nonessential amino acids, 1%

v/v antibiotic–antimycotic solution, and 1 U mL^{-1} insulin (all provided by Gibco, Invitrogen, Milan, Italy) until cells migrated from the tissue. At confluence, bone fragments were removed using sterile tweezers. The cells were detached by Trypsin–EDTA (Gibco) and cultured in complete culture medium (CM) (the same as described above, 2.4) or in differentiation culture medium (DM), as mean CM medium supplemented with 50 μg mL^{-1} ascorbic acid, 10 nM dexamethasone, and 10 mM β-glycerophosphate (all provided by Sigma, Milan, Italy). After ten days in culture, the purity of the cells was assessed by microscopic inspection, alkaline phosphatase (ALP) activity (data not shown) and calcium phosphate mineral deposition (von Kossa staining; data not shown). Our previously published data reported that 99% of cultured cells reported osteoblastic-like phenotype following 10 days in culture under the described conditions.[34] Cells were used between passages 3 and 6 in cultures.

2.6. Cytotoxicity assay

To exclude any toxic effects of biomaterials, primary human osteoblasts were cultured in 96-well plates (2×10^4 cells per well) in 100 μL of CM in direct contact with 0.4 mg of each biomaterial, that was previously placed on the bottom of the well. The cell cultures were incubated at 37 °C, 5% CO_2 for 2 h, a time of incubation previously verified as adequate to ensure cell adhesion.[35] At the end of incubation, cell viability was determined by the MTT (3-(4,5-dimethylthiazole-2-yl)-2,5-diphenyl tetrazolium bromide) assay. Briefly, cells were rinsed three times with phosphate buffered saline (PBS) to remove non-adherent cells and then incubated with a MTT solution (100 μL, 5 mg mL^{-1} in PBS; Merck, Darmstadt, Germany, Italy) at 37 °C for 4 h. The reaction was stopped by adding 0.01 N HCl in 10% w/v SDS. The absorbance was recorded at 620 nm using a microplate reader (MultiPlateReader VictorX2; PerkinElmer, Milan, Italy).

2.7. Alizarin staining

Primary human osteoblasts (2×10^5 cells) were cultured in direct contact with 4 mg of each biomaterial in 1 mL of CM or DM medium for 1, 7, or 14 days, time points previously set for calcium deposition in human primary osteoblasts.[36] The cells were washed in distilled water to remove biomaterials and samples were stained with 40 mM Alizarin red (pH 4.2) for 40 min in darkness at room temperature. The samples were incubated at 85 °C for 10 min and centrifuged (10 min, 13 000 rpm); the pH of the supernatants was neutralized before reading the absorbance of Alizarin red at 405 nm using a microplate reading (MultiPlateReader VictorX2).

2.8. RNA extraction and quantitative polymerase chain reaction (qPCR)

Primary human osteoblasts (2×10^5 cells) were cultured in direct contact for 24 h[37] with 4 mg of each biomaterial in 1 mL of CM or DM medium. The time of culture was set in previous experiments. Total RNA was extracted from cells attached to the biomaterials using the SV Total RNA Isolation System kit (Promega, Milan, Italy). Contaminating DNA was removed by DNase I digestion; 5 μg of total RNA were used to generate randomly primed cDNAs with Moloney murine leukemia virus reverse transcriptase (Applied Biosystems, Milan, Italy). Quantitative real-time polymerase chain reaction (qPCR) was performed using an ABI Prism 7700 sequence detector (Applied Biosystems) for 40 cycles at 60 °C of annealing temperature. Reactions were carried on using TaqMan Universal PCR Master Mix and Universal Probe Library (Roche, Milan, Italy), having a fluorescent dye, according to the manufacturer's instructions. Expression of the target genes was normalized to the endogenous control gene, the human glyceraldehyde-3-phosphate dehydrogenase (*GAPDH*). Data were normalized using the $2^{-\Delta\Delta CT}$ methods and are reported as fold change over osteoblasts cultured on cell-treated plastic surface. The oligonucleotide sequences and probe are listed in Table 2.

Table 2 Oligonucleotide sequences of genes evaluated by qPCR

Gene	Sequence
GAPDH	Fw: 5′-CGGGAAGCCCATCACCA-3′ Rv: 5′-CCGGCCTCACCCCATT-3′
SPP1	Fw: 5′-CGCAGACCTGACATCCAGTA-3′ Rv: 5′-GGCTGTCCCAATCAGAAGG-3′
RUNX2	Fw: 5′-CAGTGACACCATGTCAGCAA-3′ Rv: 5′-GCTCACGTCGCTCATTTTG-3′

Fw, forward; Rv, reverse; GAPDH: human glyceraldehyde-3-phosphate dehydrogenase; SSP1: secreted phosphoprotein 1; RUNX2: Runt-related transcription factor 2.

2.9. Proliferation assay

Primary human osteoblasts were incubated at 37 °C for 10 min in prewarmed PBS containing 0.1% vol/vol BSA (Merck) and 25 mM carboxyfluorescein diacetate succinimidyl ester (CFSE, Molecular Probe, Invitrogen, Walthman, MA, US). Staining was quenched by adding 5 volumes of ice-cold culture media. Sixteen h later, the cells were washed, counted using Trypan blue, and seeded at 2×10^5 cells per well in direct contact with 4 mg of each biomaterial in CM or DM medium. Cells were cultured at 37 °C, 5% CO_2 for 7 days, a time previously identified as optimal for primary human osteoblast proliferation using the CFSE probe.[38] The time of incubation was set in previous experiments. Cell proliferation was evaluated by the partitioning of CFSE fluorescent dye between daughter cells using BD FACS-Calibur flow cytometer.

2.10. Migration assay

Primary human osteoblasts were labelled for 10 min at 37 °C with 5 mM 6-carboxyfluorescein diacetate (6-CFDA, Molecular Probe, Invitrogen), a cell-permeable esterase substrate. Following a previously set protocol,[38] cells (2×10^5 cells) were seeded for 7 days in 1 mL of CM or DM medium into *trans*-well inserts (8 μm pore size, Corning, the Netherlands), held in 12-well tissue culture plates. Four mg of each biomaterial were positioned on the bottom of the wells. The media were renewed every 2 days. At the end of the incubation, the bottom side of the *trans*-well inserts was washed twice, and the cells were

harvested using cell scrapers. The cell membrane was dissolved in PBS containing 0.5% vol/vol Triton X-100. The samples were then centrifuged at 4 °C, 13 000 rpm for 10 min. Fluorescence was detected in the supernatant at excitation and emission wavelengths of 485 and 530 nm, respectively (Hitachi F2000 Fluorescence Spectrophotometer, Japan).

2.11. Statistical analysis

All biological experiments were performed at least three times with triplicate determinations for each condition. Data are reported as mean ± standard error. Statistical analysis was performed using GraphPad Prism 3.03 (San Diego, California, USA) and one-way analysis of variance followed by Bonferroni's multiple comparison tests. The normal distribution of biological data was ascertain using the Shapiro-Wilk test. Data were considered statistically different for a p value < 0.05.

3. Results

3.1. Morphological characterization

BO-L and BO-S granules presented the morphology of bovine compact bone, characterized by the presence of fracture planes with well-defined edges, large pores with a diameter included in a range of 30–300 μm, and small pores with a diameter of around 1 μm (Fig. 1). A rough surface on all the exposed faces of the examined granules was visible. As regards the pulverized form of BO, *i.e.* BO-Lp (Fig. 1E and F) and BO-Sp (Fig. 1G and H), the same surface morphology was maintained.

SB-L (Fig. 2A and B) and SB-S (Fig. 2C and D) were formed by cylindrical structures, partly maintaining the 3D printed original scaffold morphology.

SB-p samples were characterized by smaller and multiform granules (Fig. 2G and H), similar to pulverized BO granules, with well-defined edges and an irregular and rough surface.

At higher magnification, SB-L, SB-S and SB-p samples presented multiple agglomerations of small polyhedral grains of heterogeneous shape and size in the range of 2–3 μm (Fig. 3A).

SF-L granules exhibited interconnected pores in the 300–500 μm range (Fig. 2G), similar to BO-L granules. At higher magnification, the irregular and grainy surface appeared to be characterized by numerous wrinkles and cracks (Fig. 2H).

SF-S (Fig. 2I and L) had the same morphological characteristics of the larger granules of the same material; at the lower magnification they looked similar to the BO-S granules. Compared to the larger granules (SF-L), the macropores were still visible, despite being less numerous. SF-p samples (Fig. 2M and N) resembled the pulverized forms derived from the other materials. At higher magnification both sphene scaffolds and sphene foams (Fig. 3B and C, respectively) show a rough surface, where grains are visible manly in powders deriving from 3D printed scaffolds.

The EDS spectra for all the BO samples showed the presence of Ca, O and P, with relative intensity confirming the hydroxyapatite stoichiometric composition. Pulverized BO samples (*i.e.* BO-Sp and BO-Lp) exhibited higher oxygen content compared to BO-S and BO-L. The EDS spectra for both SB and SF samples of all sizes confirmed the presence of Ca, Ti, Si and O compatible with $CaO{\cdot}TiO_2{\cdot}SiO_2$ composition. The presence of the C peak can be attributed to contamination during grinding and handling operations (Fig. 4).

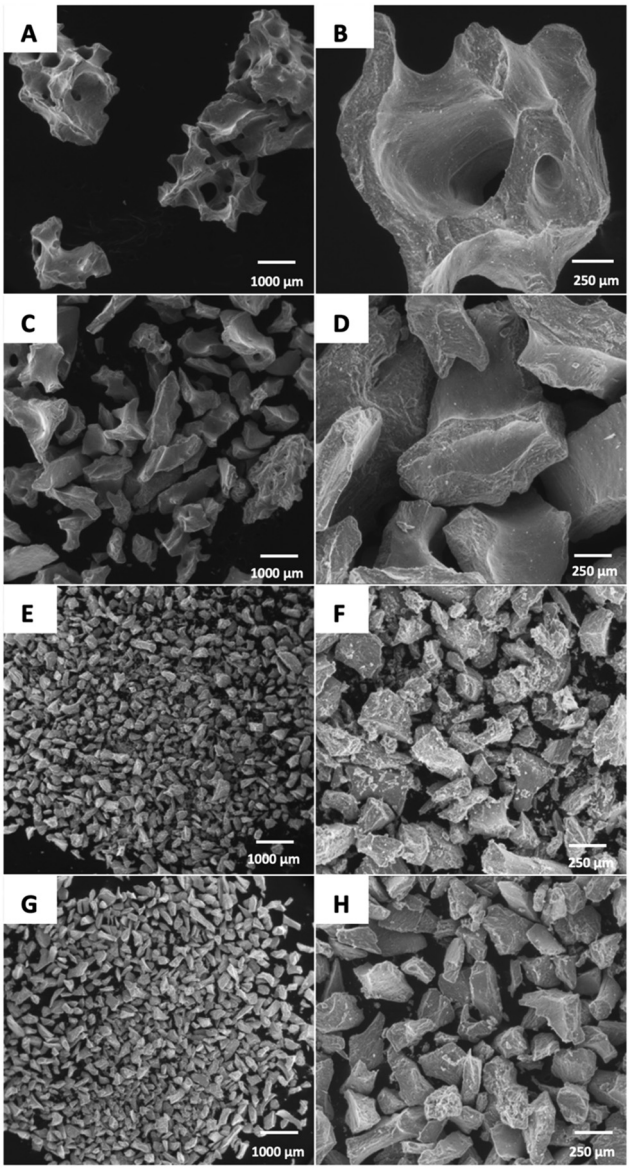

Fig. 1 SEM images of the investigated Bio-oss® granules: (A) and (B) large (BO-L); (C) and (D) small (BO-S); (E) and (F) pulverized from BO-L (BO-Lp); (G) and (H) pulverized from BO-S (BO-Sp).

For all sizes, BO samples presented negligible differences for any of the parameters evaluated by N_2 physisorption; this was clearly visible from the superimposition of the adsorption isotherms of the BO samples shown in Fig. 5.

The graph evidences that the isotherm shape is in all cases attributable to a type IV curve, typical of a mesoporous solid. There is also a small fraction of micropores, as demonstrated by the steep rise of the curve at low relative pressures ($P/P_0 < 0.1$).

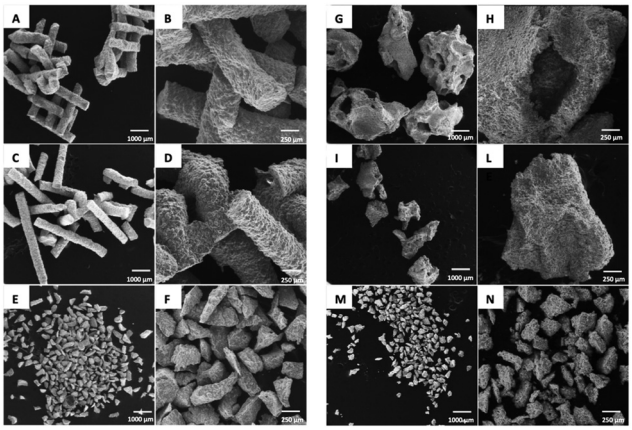

Fig. 2 SEM images of the investigated granules derived from 3D printed sphene blocks: (A) and (B) large (SB-L); (C) and (D) small (SB-S); (E) and (F) pulverized (SB-p); SEM images of sphene foam blocks: (G) and (H) large (SF-L); (I)–(L) small (SF-S); (M) and (N) pulverized (SF-p).

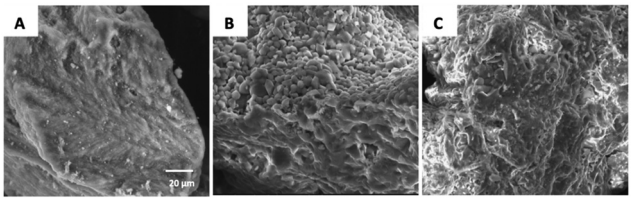

Fig. 3 High magnification SEM images of the investigated granules derived from BioOss® (A), sphene scaffolds (B) and sphene foam blocks (C).

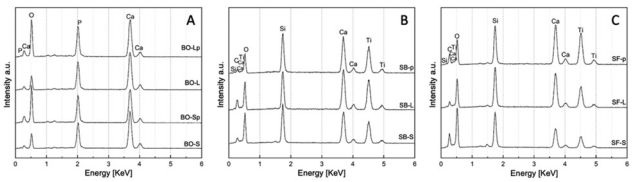

Fig. 4 EDS spectra of the investigated materials: (A) Bio-oss® (BO); (B) 3D printed sphene blocks (SB); (C) sphene foam blocks (SF). For details of acronyms see Table 1.

The H3 type hysteresis is typical of slit-shaped mesopores, while the absence of the plateau at high pressures normally results from the presence of macropores with dimensions greater than 200 nm.

The adsorption isotherms of the samples derived from the sphene bioceramic are presented in Fig. 6. Gas adsorption is negligible and, in turn, the specific surface area is lower than the detection limit. The only sphene sample showing positive adsorption values (Table 3) is the SB-p, however, this value is very close to the detection limit; hence it is affected by a very large uncertainty (around 30% on the basis of the total surface area in m^2 in the cell, according to the specifications of Micromeritics).[39]

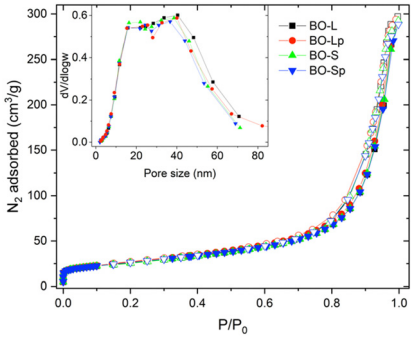

Fig. 5 Isotherms of Bio-oss® granules large (BO-L); small (BO-S); pulverized from BO-L (BO-Lp) and from BO-S (BO-Sp). Open symbols are for desorption. The inset graph represents the pore size distribution, evaluated using the BJH model in desorption.

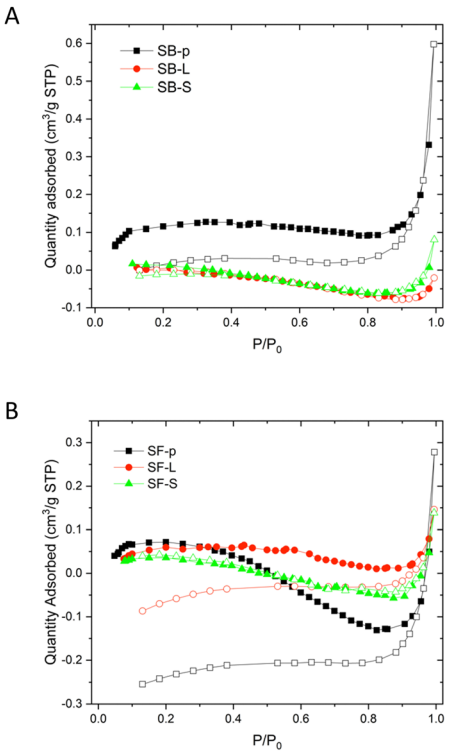

Fig. 6 Isotherms obtained from sphene derived samples showing negligible or no gas adsorption. (A) Granules derived from 3D printed sphene blocks: large (SB-L); small (SB-S); pulverized (SB-p). (B) Granules from sphene foam blocks: large (SF-L); small (SF-S); pulverized (SF-p).

3.2. Inductively coupled plasma mass spectrometry (ICP-MS)

The analysis of the culture medium (control) showed the presence of Ca, P, K, Na, and Mg in the concentrations reported in the certificate analysis of the solution provided by the manufacturer. As expected, Ti and Si were absent (Fig. 7–9).

The Ca release kinetics appeared to depend on the type of biomaterial and on the incubation time.

The presence of BO in the culture medium caused a reduction in calcium concentration starting from the first

Table 3 Relevant parameters derived from N2 physisorption measurements. The value labelled as n.a. cannot be determined owing to non-adsorbing medium (negative or too low adsorption values). For details of acronyms see Table 1

Sample	Weight[a] [g]	BET SSA[a] [$m^2\ g^{-1}$]	Total pore volume[b] [$cm^3\ g^{-1}$]	Meso-pore volume [$cm^3\ g^{-1}$]	Micro-pore volume[c] [$cm^3\ g^{-1}$]	Pore size (*meso*-pores)[d] [nm]	Pore size (micropores)[e] [nm]
BO-L	0.1681	93	0.412	0.405	0.00673	10–60	0.53
BO-Lp	0.2869	96	0.409	0.402	0.00749	10–60	0.55
BO-S	0.1530	92	0.404	0.397	0.00706	10–60	0.52
BO-Sp	0.1117	93	0.418	0.411	0.00734	10–60	0.50
SB-L	1.1872	n.a.	n.a.	n.a.	n.a.	n.a.	n.a.
SB-S	1.0703	n.a.	n.a.	n.a.	n.a.	n.a.	n.a.
SB-p	0.6038	0.40	0.000513	0.000513	n.a.	n.a.	n.a.
SF-L	0.7511	n.a.	n.a.	n.a.	n.a.	n.a.	n.a.
SF-S	0.7786	n.a.	n.a.	n.a.	n.a.	n.a.	n.a.
SF-p	0.4902	n.a.	n.a.	n.a.	n.a.	n.a.	n.a.

[a] Estimated using the BET model. [b] Measured at P/P_0 0.98. [c] From *t*-plot. [d] From BJH on desorption. [e] From Horwath–Kawazoe model.

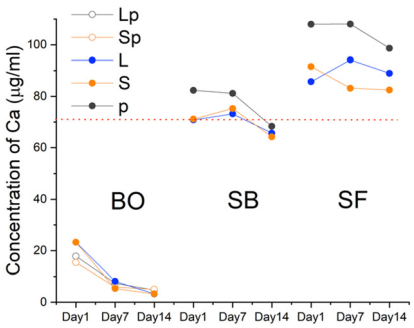

Fig. 7 ICP-MS quantification of Ca in the cell culture medium at 1, 7 and 14 days after incubation of the biomaterials. Standard error equal to 5% for all values. BO: Bio-Oss®; SB: 3D printed sphene blocks; SF: sphene foam blocks. L: large granules; S: small granules; p: pulverized granules (Lp and Sp: pulverized from BO-L and BO-S, respectively). Red dotted line = control.

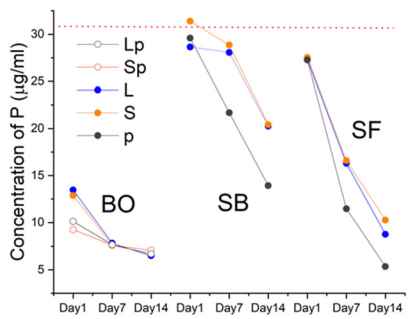

Fig. 8 ICP-MS quantification of P in the cell culture medium at 1, 7 and 14 days after incubation of the biomaterials. Standard error equal to 10% for all values. BO: Bio-Oss®; SB: 3D printed sphene blocks; SF: sphene foam blocks. L: large granules; S: small granules; p: pulverized granules (Lp and Sp: pulverized from BO-L and BO-S, respectively). Red dotted line = control.

day. The decline continued sustained until day 7 and a further reduction occurred at 14 days, albeit less noticeable. In the

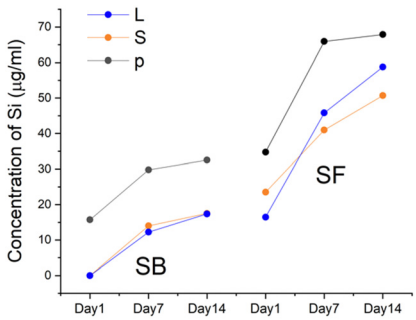

Fig. 9 ICP-MS quantification of Si in the cell culture medium at 1, 7 and 14 days after incubation of the biomaterials. Standard error equal to 15% for all values. BO: Bio-Oss®; SB: 3D printed sphene blocks; SF: sphene foam blocks. L: large granules; S: small granules; p: pulverized granules (Lp and Sp: pulverized from BO-L and BO-S, respectively).

presence of SB, values remained similar to the control solution. On the contrary, in presence of SF the level of Ca in the culture medium increased on day 1. SF-p showed the highest levels of Ca released at all the evaluated time points.

The P content showed a trend analogous to Ca for all the BO granules. All forms of sphene granules showed a considerable absorption after 14 days, particularly for SB-p and SF-p.

ICP-MS was also used to determine the Ti and Si content present in the culture medium in the absence and presence of the biomaterials. As expected, both elements were absent in BO. In all sphene-derived granules, the concentration of Si increased at 7 and 14 days with a similar trend; however higher values were observed for all SF granules and the highest value was recorded for SF-p. Regarding Ti, some of the measured concentrations were above the detection limit (0.006 µg mL^{-1}) on day 1, but all below the quantification limit (0.018 µg mL^{-1}) and no signal at all was present after day 1.

3.3. Cytotoxicity assay

The cytotoxic activity of different biomaterials was assessed on cultured primary human osteoblasts using the MTT assay

(Fig. 10). The ratio of the quantity of biomaterial/volume of cell culture was kept constant during all the biological experiments; it reflected the experimental conditions described in the chemical profile analysis. None of the tested biomaterials did show a cytotoxic activity as compared to control cells, *i.e.* osteoblasts seeded in cell-treated plastic plates with no biomaterial.

3.4. Alizarin staining

To evaluate the role of biomaterials in supporting matrix mineralization, we evaluated Alizarin red as a marker of matrix mineralization in primary human osteoblasts cultured for 1–14 days in CM medium. Fig. 11 reports that BO samples slightly increased Alizarin red in osteoblasts cultured for 1, 7, or 14 days. BO-Lp significantly increased Alizarin-related signals after 14 days of culture. All sphene derived granules showed results comparable to BO and no statistically different results were obtained among BO, SB, and SF at the different tested time points. Alizarin red quantification significantly increased in primary human osteoblasts cultured with SB-S and SB-L as well as with SF-L and SF-S while the latter showed the best induction effect. Matrix mineralization was evident starting from day 7 in culture and the effects persisted until day 14 (Fig. 11).

SF-p followed the mineralization feature reported for control cells, whereas SB-p reported a significant reduction in matrix mineralization on day 7, this effect disappeared after 14 days of culture.

The same experiments were performed by culturing the primary human osteoblasts in DM medium enriched with elements supporting osteoblast differentiation. Results were similar, showing that all tested materials supported matrix mineralization, independently of the incubation medium (Fig. 12).

3.5. Quantitative polymerase chain reaction (qPCR)

To confirm data reported in Alizarin red experiments, primary human osteoblasts cultured for 24 h day in either CM or DM media were subjected to RNA extraction and quantification of genes involved in osteoblast phenotype, namely osteopontin *SSP1*, coding a protein involved in binding hydroxyapatite with

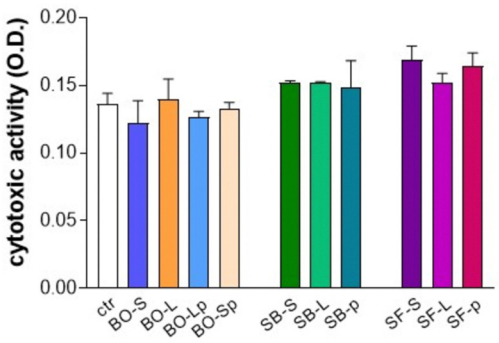

Fig. 10 Cytotoxicity assay using MTT (3-(4,5-dimethylthiazole-2-yl)-2,5-diphenyl tetrazolium bromide). Tested biomaterials did not show cytotoxic activity as compared with control (ctr). For details of acronyms see Table 1.

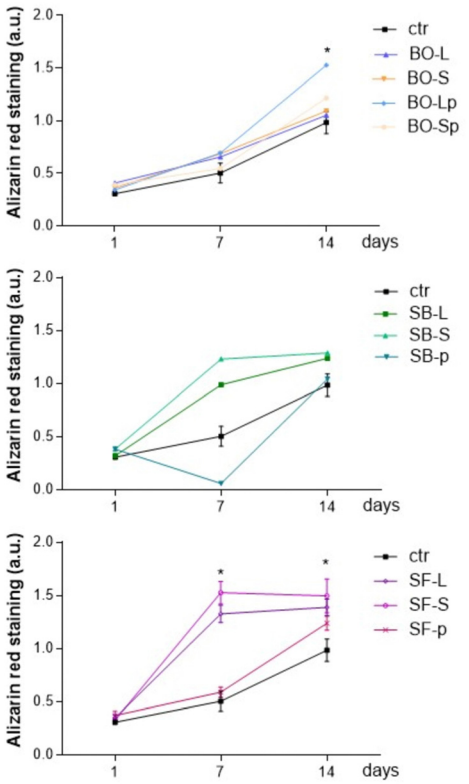

Fig. 11 Alizarin red staining test, culture medium. * $p < 0.05$ *vs.* the same biomaterial at 1 day.

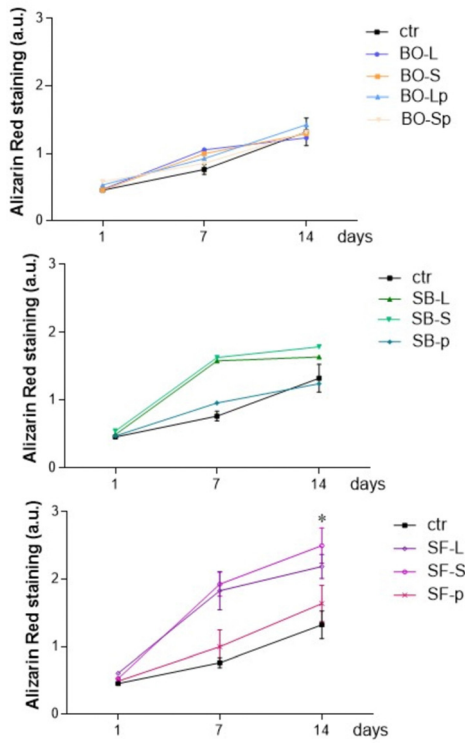

Fig. 12 Alizarin red staining test, differentiation medium. * $p < 0.05$ *vs.* the same biomaterial at 1 day. For details of acronyms see Table 1.

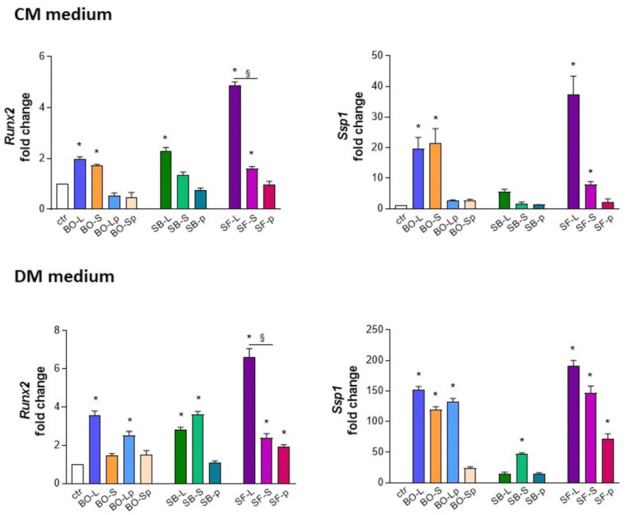

Fig. 13 RNA extraction and quantification of genes involved in primary human osteoblast phenotype, namely osteopontin SSP1, and RUNX2, in culture and differentiation medium (CM and DM, respectively). * $p < 0.05$ *vs.* control; § SF-L *vs.* SF-S $p < 0.05$. For details of acronyms see Table 1.

high affinity, and *RUNX2*, a key transcriptional modulator of osteoblast differentiation. As reported in Fig. 13, osteoblasts cultured in CM medium with BO-L, BO-S, SF-L, and SF-S increased the expression of *SSP1* and *RUNX2* mRNA transcripts. *RUNX2* transcripts increased also in cultures with SB-L. Cultures in DM medium further supported the osteogenic phenotype since BO-Lp and all tested sizes of sphene foam increased *SSP1* and *RUNX2* mRNA transcript levels. Interestingly, for differentiation medium, RUNX2 expression was significantly higher in presence of SF-L as compared to SF-S.

3.6. Proliferation and migration assay

Proliferation was assessed by evaluating the partitioning between daughter cells of CFSE probe-related fluorescence in primary human osteoblasts cultured for 7 days in CM or DM media. According to FACS analysis (Fig. 14), fluorescence partitioning occurred in 5.21% of the cells cultured on plastic surfaces. Cells cultured with BO-Lp or SB-L and SB-S significantly increased proliferation and the best performance was reported for BO-Lp cultures in DM (62.31% CFSE positive cells).

Besides increasing cellular proliferation, SB-S was the only biomaterial reporting a significantly higher increase in cell migration of osteoblasts cultured in CM medium (Fig. 15). No significant differences were observed among the tested samples in primary human osteoblast migration at 7 days in DM medium.

4. Discussion

This *in vitro* study evaluated the physico-chemical and biological properties of granules of various sizes derived from two types of sphene blocks; they were compared to the properties of deproteinized bovine bone mineral (DBBM) granules of the same size. The DBBM utilized in the present study (BO) is a

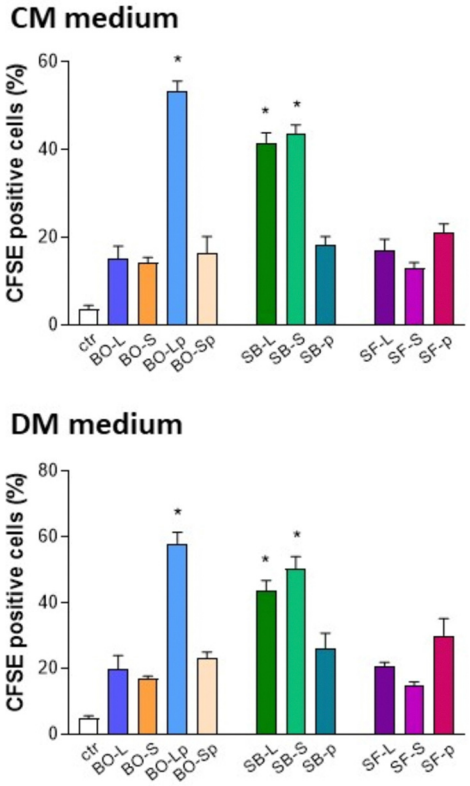

Fig. 14 Carboxyfluorescein diacetate succinimidyl ester (CFSE) test for proliferation of primary human osteoblasts cultured in culture and differentiation medium (CM and DM, respectively). * $p < 0.05$ *vs.* control. For details of acronyms see Table 1.

heavily investigated and used biomaterial which presents macroscopic and microscopic features of natural bone.[40–42]

Particle size is known to affect the osteoconductive properties and the degradation kinetics of the biomaterials;[25,43] however, the ideal particle size is still controversial. The osteoconductive properties of smaller size particles (250–1000 μm) were found to be comparable to those observed for larger ones (1000–2000 μm) of the same DBBM graft material.[16–18] Nevertheless, larger particles might be advantageous, as they leave more space for vascular ingrowth.[16]

Encouraging results have been observed in pre-clinical studies with smaller size DBBM particles, in the range of 125–250 μm (named pulverized or paste-like, with or without a carrier).[26,27] Pulverized particle grafts are indicated in non-containing periodontal defects because of their easy handling properties and improved mechanical stability, for crestal or buccal bone regeneration as for socket preservation. These features seem particularly favourable in the presence of a thin periodontal phenotype as they limit or even avoid the risk of migration or exfoliation of larger graft particles through the healing soft tissues.[28–32]

In the current study, all pulverized granules showed similar morphology. Furthermore, non-pulverized SF granules presented some similarities to natural bone in terms of geometry and macro-porosity. Determining the distribution and size of

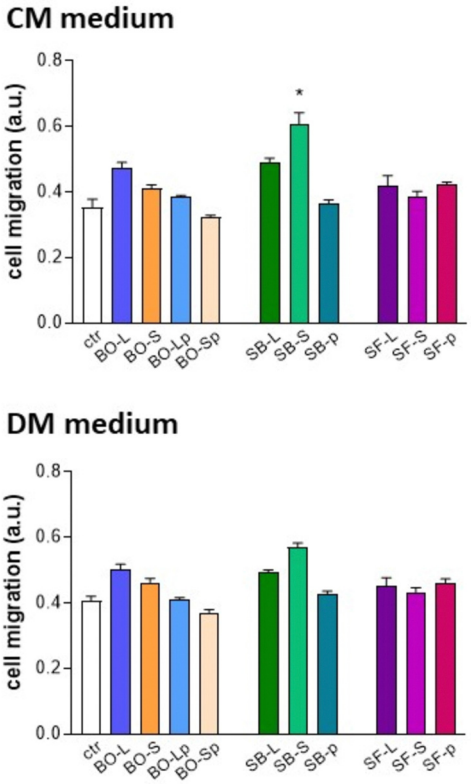

Fig. 15 Migration test of primary human osteoblasts cultured in culture and differentiation medium (CM and DM, respectively). * $p < 0.05$ *vs.* control. For details of acronyms see Table 1.

the pores obtained using the BHJ model describes a mesoporous material for all sizes of the BO granules. The microstructure of both SB-L and SF-L still reflects some residual macroporosity derived from the process, whilst both SB-S and SF-S maintain the fragments of the solid part of the structure. Indeed, SB-S exhibited cylindrical fragments derived from the extrusion, whereas SF-S was characterized by fragments with irregular shapes.

In a study comparing BO granules of 500–1000 μm and a synthetic HA, the specific surface area of the latter could not be measured with the Brunauer–Emmett–Teller (BET) analysis because the value was below the quantification limit of the instrument.[44] The same study using quantitative histomorphometric analysis demonstrated that BO displayed significantly higher newly formed bone compared to the synthetic HA. In the current study, sphene granules presented undetectable values for specific surface area and porosity, with the exception of SB-p. On the other hand, the SEM observation showed macropores and cracks on the sphene granules; consequently, it can be assumed that sphene surface characteristics may promote superficial protein adsorption, including bone morphogenetic proteins (BMPs)[45] and stimulate cell adhesion and bone tissue growth.[46–52] All the investigated materials showed progressive absorption of P; it was more evident for all forms of BO and for the sphene pulverized granules. As for BO, the decrease of Ca and P in the cell culture medium suggests that this biomaterial can alter the physiological levels of these elements which are considered crucial to the function of osteoblasts, for gene expression of osteogenic cells, as well as for the mineralization of newly formed bone.[53–55] The absorption of Ca and P on BO particles was also observed at ICP experiments by Mladenović *et al.*,[56] who further confirmed the uptake of Ca on BO surface with radioactive calcium-45 isotope labelling technique. In our experiments, we reported that the expression of *RUNX2* and *SSP1* are higher in primary human osteoblasts cultured for 1 day in BO-L and BO-S (Fig. 13), which less sequester P and Ca as compared with pulverized biomaterials, which reported increased avidity for the elements. The correlation between bioavailability of soluble elements and gene expression profile appears biomaterial-dependent as the effects are at the opposite in osteoblast cultured on sphene. In another study of our group investigating the ions release kinetics of 3D printed sphene ceramic scaffolds, a rapid release of Ca in PBS was observed within the first hours after soaking.[9] In the present investigation, the sphene samples tended to release Ca in the culture medium and not to absorb it. This phenomenon was more pronounced in the SF groups. The dissolution of Ca from sphene scaffolds can be partially explained as a consequence of its crystal structure, which allows for some diffusion of the embedded Ca ions.[9]

The concentrations of Si in the culture medium increased overtime in all sphene groups, especially between day 1 and 7. For both SB and SF, the highest Ca and Si concentrations were detected at all time points with the pulverized forms. The release of Si observed from sphene granules might *in vivo* be correlated to bone health.[15] Concentrations of $Si(OH)_4$ ranging from 10 to 1000 μM have been demonstrated to increase the proliferation of human osteoblast-like cells.[57] The ability to release Si in solution provides osteoinductive properties to the silicate bioceramics. In particular, biomaterials capable of releasing Si have the ability to stimulate the proliferation of osteoblasts, induce angiogenesis and formation of bone tissue.[58]

As regards the release of Ti ions from sphene samples, in previous investigations of our group sphene coatings revealed to be chemically stable in Tris–HCl and only trace amount of Ti ions could be detected in the solution after immersion up to 7 days.[13] Similarly, the concentration of Ti ions released by 3D printed sphene scaffolds was below the detection limit of the ICP device utilized (<0.01 mg L^{-1}), which is lower than the usual Ti concentration in humans (0.2 mg L^{-1}).[9] In line with these findings, in the present study the concentration of Ti ions released by sphene scaffolds was always below the quantification limit (0.018 μg mL^{-1}), independently of the time point, the production method and the size of the granules. No group showed cytotoxicity and all were able to induce matrix mineralization *in vitro*, independently of the medium. Among BO granules, BO-Lp showed the best results that were alike to SF-S. The qPCR results were similar for all the granule types. The granules of the same dimension displayed a similar pattern of expression but SF-L provided always the highest results. Cells migration was observed on all tested materials, thus supporting

cell colonization of the grafts. Interestingly, BO-Lp, SB-L and SB-S granules were associated with an increased proliferation, both in differentiated and undifferentiated media. Our present data are in line with the absence of cytotoxicity of Bio-Oss® as previously demonstrated.[40–42]

In an *in vitro* study investigating the impact of bone substitute granule size on osteoblast behaviour,[59] the larger BO granules presented significantly increased viability values on day 3 compared to the smaller granules. Whereas, higher mRNA levels of *RUNX2* at 14 days and osteocalcin (*OCN*) at 3 and 14 days were observed for human osteosarcoma cell line SaOS-2 cultured onto small BO granules than onto larger ones.

As to the antibacterial properties, the tested biomaterials did not interfere with the growth of microbial species commonly found in the oral cavity. Our experiments reported that *Streptococcus* spp. developed a biofilm independently of the size, porosity or chemical composition of the granules. The absence of antibacterial activity of pure BO has also been demonstrated in studies primarily aiming at investigating the enrichment of this biomaterial with antimicrobial agents, such as silver-doped hydroxyapatite (AgHA)[60] or tetracycline hydrochloride.[61] These studies were performed using commercially available BO granules, while, to the best of our knowledge, this is the first work to report information about the antimicrobial properties of the pulverized form.

The results obtained for the sphene granules corroborate previous *in vitro* and *in vivo* studies conducted by our group. As a sphene ceramic coating, it was shown to support mesenchymal stem cell adhesion and proliferation.[13] Furthermore, the biocompatibility and osseointegration of sphene-coated titanium implants were demonstrated in a rat femur model.[14] Simulated body fluid and cell culture tests also confirmed the bioactivity and the cytocompatibility of 3D sphene ceramic scaffold obtained *via* the polymer derived ceramics route and printed by means of DIW, as the SB samples used in the present work.[9] Overall, this bioceramic seems to satisfy the requirements for an effective osteoconduction.

One concern about the use of biomaterials in different sizes could be the immunological reaction against the granule size *in vivo*. Previous histological findings of studies investigating pulverized BO[26,27] showed that new bone formation and integration of the bovine graft particles in bone were achieved in animal models, without qualitative differences between pulverized, small, and large particles. Moreover, the resorptive activity was not enhanced, and no immunological reaction was visible. In a prospective clinical histomorphometric study on sinus floor augmentation using large or small bovine bone mineral particles, Chackartchi *et al.*[17] reported that in both groups the osteoclast-like cells preferred the small-size bovine bone particles and not the large particles. No inflammatory cell infiltrate was present around the particles or at the bone interface.[17] Leiblen *et al.*[62] studied the effect of granule size of a bone graft substitute (Herafill®, calcium sulfate, combined with calcium carbonate, triglyceride, and gentamicin) on bone healing using Masquelet's induced membrane in a critical size defect model in the rat femur. Three different ranges of granule sizes of Herafill® were used as a scaffold (0.5–1 mm, 1–3 mm, 3–5 mm). Granules of the 0.5–1.0 mm range showed a significantly improved bone healing compared to larger granule sizes. Another study demonstrated clear differences between the S- and L-size of BO granules in the material surface area, cell viability, and differentiation potential both in macrophage and osteoblasts, suggesting that the higher surface area of the S-size granules might enlarge the cell adhesion area and promote differentiation more efficiently than that of the BO-L granules.[59]

For the sphene, some evidence is available about the possible immunological response to this biomaterial. Indeed, in the knee joints corresponding to the side where sphene-coated implants had been positioned, no synovial fluid could be collected both after 14 and 28 days following implant placement in the rat femurs; this confirmed the absence of local inflammation.[14] However, more immunological studies comparing the effect of different biomaterials and granule sizes are lacking in order to provide a deeper insight into these aspects.

The absence of *in vivo* experiments could be considered the main limitation of the present study. Moreover, the use of granules obtained from 3D printed blocks could represent a stretch, since they are not meant to be produced for this purpose, but they are generally manufactured in blocks to precisely match a specific bone defect. Commercially available BO-L and BO-S are sterilized by gamma irradiation by the manufacturer. However, to guarantee the sterility of the BO pulverized granules for biological and microbiological tests, BO-Lp and BO-Sp were sterilized by steam autoclaving similarly to the sphene samples. This might have affected the properties of the materials. Nevertheless, the same sterilization process has been frequently reported as a standard in similar *in vitro* studies, when gamma irradiation is not available.[63–65] Furthermore, the microbiological data we obtained need to be interpreted with caution, as the *in vitro* experiments do not take into consideration the complex environment of the oral mucosa (saliva, mucin, diet derived elements, microbiota). Although Alizarin red experiments were performed at multiple time points, PCR test was performed just after one day of cell culture. Even if the time of incubation for the PCR analysis was decided based on the previous time course experiments, it would be interesting to investigate the time-dependent expression of other osteoblast markers to better understand the influence of different biomaterials and granule sizes on osteoblast gene expression profile. To be complete, the *in vitro* behavior of other cells involved in bone regeneration, such as endothelial cells or stem cells, could also be explored. Future developments include *in vivo* preclinical studies, in order to investigate the safety, the resorbability and the osteoconductive properties of these biomaterials, with the final goal of converting these bone substitutes into clinical products.

5. Conclusions

This *in vitro* study demonstrated that sphene granules obtained from different processing conditions have biological

characteristics similar to deproteinized bovine bone, the grafting material widely used in clinical practice. Variations in the size of both sphene and bovine bone granules did not modify their physico-chemical and biological properties, whereas the pulverized form of bovine bone increased the osteoblastic response *in vitro*.

Author contributions

Stefano Sivolella: conceptualization; data curation; writing – original draft; writing – review & editing; supervision; project administration. Giulia Brunello: data curation; writing – original draft; writing – review & editing. Ervin Nika: investigation; writing – review & editing. Denis Badocco: investigation; formal analysis; writing – review & editing. Paolo Pastore: investigation; formal analysis; writing – review & editing. Sara M. Carturan: investigation; formal analysis; writing – review & editing. Enrico Bernardo: writing – review & editing. Hamada Elsayed: investigation; formal analysis; writing – review & editing. Lisa Biasetto: conceptualization; data curation; supervision; writing – review & editing. Paola Brun: conceptualization; investigation; formal analysis; data curation, writing – review & editing.

Conflicts of interest

The authors declare no conflict of interest associated with this article.

Notes and references

1 V. L. Zizzari, S. Zara, G. Tetè, R. Vinci, E. Gherlone and A. Cataldi, *Oral Surg. Oral Med. Oral Pathol. Oral Radiol.*, 2016, **122**, 392–402.
2 A. Assari, M. Hani, H. Qaid, B. Omar and L. Aleid, *J. Stomatol. Oral Maxillofac Surg.*, 2022, **123**, e563–e568.
3 C. Bucchi, M. Del Fabbro, A. Arias, R. Fuentes, J. M. Mendes, M. Ordonneau, V. Orti and M. C. Manzanares-Céspedes, *Patient Prefer Adherence*, 2019, **13**, 179–185.
4 C. Vaquette, J. Mitchell and S. Ivanovski, *Front. Bioeng. Biotechnol.*, 2021, **9**, 798393.
5 G. Brunello, S. Sivolella, R. Meneghello, L. Ferroni, C. Gardin, A. Piattelli, B. Zavan and E. Bressan, *Biotechnol. Adv.*, 2016, **34**, 740–753.
6 C. Wu and J. Chang, *Biomed. Mater.*, 2013, **8**, 032001.
7 D. Yi, C. Wu, B. Ma, H. Ji, X. Zheng and J. Chang, *J. Biomater. Appl.*, 2014, **28**, 1343–1353.
8 G. Brunello, H. Elsayed and L. Biasetto, *Materials*, 2019, **12**, 2929.
9 H. Elsayed, M. Sayed, S. M. Naga, P. Rebesan, C. Gardin, Z. Zavan, P. Colombo and E. Bernardo, *J. Eur. Ceram. Soc.*, 2022, **42**, 286–295.
10 H. Elsayed, A. Zocca, G. Franchin, E. Bernardo and P. Colombo, *J. Eur. Ceram. Soc.*, 2016, **36**, 829–835.
11 C. Wu, Y. Ramaswamy, A. Soeparto and H. Zreiqat, *J. Biomed. Mater. Res., Part A*, 2008, **86**, 402–410.
12 Y. Ramaswamy, C. Wu, C. R. Dunstan, B. Hewson, T. Eindorf, G. I. Anderson and H. Zreiqat, *Acta Biomater.*, 2009, **5**, 3192–3204.
13 H. Elsayed, G. Brunello, C. Gardin, L. Ferroni, D. Badocco, P. Pastore, S. Sivolella, B. Zavan and L. Biasetto, *Materials*, 2018, **11**, 2234.
14 G. Brunello, L. Biasetto, H. Elsayed, E. Sbettega, C. Gardin, A. Scanu, S. Carmignato, B. Zavan and S. Sivolella, *J. Clin. Med.*, 2020, **9**, 1290.
15 W. Götz, E. Tobiasch, S. Witzleben and M. Schulze, *Pharmaceutics*, 2019, **11**, 117.
16 T. Testori, S. S. Wallace, P. Trisi, M. Capelli, F. Zuffetti and M. Del Fabbro, *Int. J. Periodontics Restorative Dent.*, 2013, **33**, 467–475.
17 T. Chackartchi, G. Iezzi, M. Goldstein, A. Klinger, A. Soskolne, A. Piattelli and L. Shapira, *Clin. Oral. Implants Res.*, 2011, **22**, 473–480.
18 S. S. Jensen, M. Aaboe, S. F. Janner, N. Saulacic, M. M. Bornstein, D. D. Bosshardt and D. Buser, *Clin. Implant Dent. Relat. Res.*, 2015, **17**, 274–285.
19 S. Sayardoust, W. Norstedt and F. A. Shah, *Clin. Exp. Dent. Res.*, 2022, **8**, 640–649.
20 A. Martinez, O. Balboa, I. Gasamans, X. L. Otero-Cepeda and F. Guitian, *Clin. Oral. Implants Res.*, 2015, **26**, 623–632.
21 N. D. MacBeth, N. Donos and N. Mardas, *Clin. Oral. Implants Res.*, 2022, **33**, 681–699.
22 A. Kolk, J. Handschel, W. Drescher, D. Rothamel, F. Kloss, M. Blessmann, M. Heiland, K. D. Wolff and R. Smeets, *J. Craniomaxillofac Surg.*, 2012, **40**, 706–718.
23 J. Becker, B. Al-Nawas, M. O. Klein, H. Schliephake, H. Terheyden and F. Schwarz, *Clin. Oral. Implants Res.*, 2009, **20**, 742–749.
24 F. Schwarz, A. Hegewald, N. Sahm and J. Becker, *Clin. Oral. Implants Res.*, 2014, **25**, 1010–1015.
25 V. Karageorgiou and D. Kaplan, *Biomaterials*, 2005, **26**, 5474–5491.
26 D. Busenlechner, S. Tangl, C. Fitzl, T. Bernhart, R. Gruber and G. Watzek, *Clin. Oral. Implants Res.*, 2009, **20**, 1099–1104.
27 A. Ivanovic, D. D. Bosshardt, I. Mihatovic, F. Schwarz, R. Gruber and A. Sculean, *Clin. Oral. Investig.*, 2014, **18**, 1319–1328.
28 M. Hallman and A. Thor, *Periodontol 2000*, 2008, **47**, 172–192.
29 M. Schlee and M. Esposito, *Eur. J. Oral Implantol*, 2009, **2**, 209–217.
30 H. H. Takei, T. J. Han, F. A. Carranza, Jr., E. B. Kenney and V. Lekovic, *J. Periodontol.*, 1985, **56**, 204–210.
31 G. Steiner, After Mineralization, Mineralized Freeze-Dried Bone Allograft Particles Are Exfoliated but not Resorbed., **https://www.preprints.org/manuscript/201904.0271/v1**, (accessed 09 September, 2022).
32 R. B. Santana and C. M. de Mattos, *Int. J. Oral Maxillofac Implants*, 2009, **24**, 81–87.

33 S. Chalk and L. McEwen, *Chem. Int.*, 2017, **39**, 25–30.
34 A. Bagno, A. Piovan, M. Dettin, P. Brun, R. Gambaretto, G. Palù, C. Di Bello and I. Castagliuolo, *Bone*, 2007, **41**, 704–712.
35 P. Brun, M. Scorzeto, S. Vassanelli, I. Castagliuolo, G. Palù, F. Ghezzo, G. M. Messina, G. Iucci, V. Battaglia, S. Sivolella, A. Bagno, G. Polzonetti, G. Marletta and M. Dettin, *Acta Biomater.*, 2013, **9**, 6105–6115.
36 P. Brun, F. Ghezzo, M. Roso, R. Danesin, G. Palù, A. Bagno, M. Modesti, I. Castagliuolo and M. Dettin, *Acta Biomater.*, 2011, **7**, 2526–2532.
37 M. Dettin, A. Zamuner, M. Roso, A. Gloria, G. Iucci, G. M. Messina, U. D'Amora, G. Marletta, M. Modesti, I. Castagliuolo and P. Brun, *PLoS One*, 2015, **10**, e0137505.
38 A. Zamuner, E. Zeni, H. Elsayed, M. Di Foggia, P. Taddei, A. Pasquato, L. Di Silvio, E. Bernardo, P. Brun and M. Dettin, *Biomimetics*, 2023, **8**, 185.
39 Micromeritics, Minimum Surface Area Measurements with Micromeritics Physisorption Analyzers, **https://www.micromeritics.com/Repository/Files/micro_tech_tip_14-surface-area-analyses.pdf**, (accessed 28 December 2022).
40 C. R. Dumitrescu, I. A. Neacsu, V. A. Surdu, A. I. Nicoara, F. Iordache, R. Trusca, L. T. Ciocan, A. Ficai and E. Andronescu, *Nanomaterials*, 2021, **11**, 2289.
41 A. Bernhardt, A. Lode, F. Peters and M. Gelinsky, *Clin. Oral. Implants Res.*, 2011, **22**, 651–657.
42 Q. Liu, T. Douglas, C. Zamponi, S. T. Becker, E. Sherry, S. Sivananthan, F. Warnke, J. Wiltfang and P. H. Warnke, *Clin. Oral. Implants Res.*, 2011, **22**, 1259–1264.
43 I. R. Zerbo, A. L. Bronckers, G. de Lange and E. H. Burger, *Biomaterials*, 2005, **26**, 1445–1451.
44 F. Lambert, M. Bacevic, P. Layrolle, P. Schüpbach, P. Drion and E. Rompen, *Clin. Oral. Implants Res.*, 2017, **28**, e201–e207.
45 H. Yuan, P. Zou, Z. Yang, X. Zhang, J. D. De Bruijn and K. De Groot, *J. Mater. Sci.: Mater. Med.*, 1998, **9**, 717–721.
46 C. M. Walthers, A. K. Nazemi, S. L. Patel, B. M. Wu and J. C. Dunn, *Biomaterials*, 2014, **35**, 5129–5137.
47 M. Rouahi, O. Gallet, E. Champion, J. Dentzer, P. Hardouin and K. Anselme, *J. Biomed. Mater. Res., Part A*, 2006, **78**, 222–235.
48 M. Rouahi, E. Champion, O. Gallet, A. Jada and K. Anselme, *Colloids Surf., B*, 2006, **47**, 10–19.
49 F. M. Klenke, Y. Liu, H. Yuan, E. B. Hunziker, K. A. Siebenrock and W. Hofstetter, *J. Biomed. Mater. Res., Part A*, 2008, **85**, 777–786.
50 M. Hulsman, F. Hulshof, H. Unadkat, B. J. Papenburg, D. F. Stamatialis, R. Truckenmüller, C. van Blitterswijk, J. de Boer and M. J. Reinders, *Acta Biomater.*, 2015, **15**, 29–38.
51 X. Li, C. A. van Blitterswijk, Q. Feng, F. Cui and F. Watari, *Biomaterials*, 2008, **29**, 3306–3316.
52 A. M. Barradas, H. Yuan, C. A. van Blitterswijk and P. Habibovic, *Eur. Cells Mater.*, 2011, **21**, 407–429; discussion 429.
53 S. Khoshniat, A. Bourgine, M. Julien, M. Petit, P. Pilet, T. Rouillon, M. Masson, M. Gatius, P. Weiss, J. Guicheux and L. Beck, *Bone*, 2011, **48**, 894–902.
54 M. M. Dvorak, A. Siddiqua, D. T. Ward, D. H. Carter, S. L. Dallas, E. F. Nemeth and D. Riccardi, *Proc. Natl. Acad. Sci. U. S. A.*, 2004, **101**, 5140–5145.
55 A. T. Xu, W. T. Qi, M. N. Lin, Y. H. Zhu and F. M. He, *J. Biomed. Mater. Res., Part B*, 2020, **108**, 272–281.
56 Ž. Mladenović, A. Sahlin-Platt, B. Andersson, A. Johansson, E. Björn and M. Ransjö, *Clin. Oral. Implants Res.*, 2013, **24**, 329–335.
57 M. Wiens, X. Wang, H. C. Schröder, U. Kolb, U. Schlossmacher, H. Ushijima and W. E. Müller, *Biomaterials*, 2010, **31**, 7716–7725.
58 W. Zhai, H. Lu, L. Chen, X. Lin, Y. Huang, K. Dai, K. Naoki, G. Chen and J. Chang, *Acta Biomater.*, 2012, **8**, 341–349.
59 M. Fujioka-Kobayashi, H. Katagiri, M. Kono, B. Schaller, T. Iizuka and A. F. Safi, *Clin Oral Investig*, 2021, **25**, 4949–4958.
60 J. Gong, L. Yang, Q. He and T. Jiao, *J. Biomed. Mater. Res., Part B*, 2018, **106**, 410–420.
61 A. Dashti, D. Ready, V. Salih, J. C. Knowles, J. E. Barralet, M. Wilson, N. Donos and S. N. Nazhat, *J. Biomed. Mater. Res., Part B*, 2010, **93**, 394–400.
62 M. Leiblein, E. Koch, A. Winkenbach, A. Schaible, C. Nau, H. Büchner, K. Schröder, I. Marzi and D. Henrich, *J. Biomed. Mater. Res., Part B*, 2020, **108**, 1469–1482.
63 A. Trbakovic, P. Hedenqvist, T. Mellgren, C. Ley, J. Hilborn, D. Ossipov, S. Ekman, C. B. Johansson, M. Jensen-Waern and A. Thor, *J. Dent.*, 2018, **70**, 31–39.
64 M. M. Smith, W. J. Duncan and D. E. Coates, *J. Periodontal Res.*, 2018, **53**, 80–90.
65 S. Lymperi, V. Taraslia, I. N. Tsatsoulis, A. Samara, A. D. Velentzas, A. Agrafioti, E. Anastasiadou and E. Kontakiotis, *BioMed Res. Int.*, 2015, **2015**, 189872.